

# A Bidirectional Buck-Boost Converter-Based Switching Ripple Communication Strategy for Intelligent Street Lighting Systems

Research paper

Yixuan Zhang<sup>1,\*</sup>, Yihua Hu<sup>1</sup>, Zion Tse<sup>1</sup>, Yuwei Liu<sup>1</sup>, Jiamei Deng<sup>2</sup>, Hui Xu<sup>2</sup>, Yangang Wang<sup>3</sup>, Wei Li<sup>4</sup>

<sup>1</sup>Department of Electronics, University of York, York, United Kingdom

<sup>2</sup>Department of Artificial Intelligence, Control, and Energy, Leeds Beckett University, Leeds, United Kingdom

<sup>3</sup>Dynex Semiconductor Ltd, Lincoln, United Kingdom

<sup>4</sup>State Grid International Development Co., Ltd, Beijing, China

Received: September 18, 2021; Accepted: October 29, 2021

**Abstract:** The light-emitting diode (LED) is an essential component of intelligent street lighting (ISL) systems. An efficient ISL system can not only reduce power consumption by planning LED illuminating time but also reduce maintenance costs through a high degree of automation. In this paper, a buck-boost converter is used to realise composite transmission of power and signals for an ISL system. The power is modulated by the pulse width modulation (PWM) approach, and the switching ripple generated in the PWM process is utilised as the carrier of the signals transmitted between the remote-control centre and the slave nodes. Moreover, the proposed model involves a 'request to send (RTS)/confirm to send (CTS)' mechanism to avoid signal conflicts. Compared with the conventional power line communication (PLC) approach, the proposed transmission scheme has the advantages of simple circuit structure and simple system wiring. Additionally, a simulation model built in MATLAB/Simulink proves the designed transmission method has strong anti-noise ability.

**Keywords:** *bidirectional switching ripple communication • buck-boost converter • intelligent street lighting system • pulse width modulation • smart city*

## 1. Introduction

Street lighting systems play a vital role in road safety, citizens' daily lives, and urban beautification. As more street lights are used to satisfy the requirements of urban development, an efficient light-emitting diode (LED) management method is needed to reduce the power consumption of urban illumination systems and delay the ageing and malfunctioning of bulbs (du Toit et al., 2017; SEA, 2012).

Facing the above-mentioned design requirements, research on intelligent street lighting (ISL) systems has become more and more common in recent years. As an essential component of smart cities, ISL can promote the implementation of smart municipalities, and improve urban and municipal service capabilities. Specifically, it can achieve functions such as the current, voltage, and temperature measurement of street lights, on-site operation monitoring of important road sections, street light-based electric vehicle charging piles, and so on (Novak et al., 2014; Gu et al., 2018). In such a system, communication between the LED lights and the remote console is essential for system automation, which can reduce the cost of manual detection in the event of LED failure and promote the usability of LED lights according to actual environmental conditions (Adriansyah et al., 2017). To realise communication between LED lights and the remote console, a feasible solution is to use the framework of the Internet of Things, wherein embedded and wireless sensors such as light, sound and infrared sensors are used for LED light status detection and sampled data are transmitted to the remote control centre through various approaches such as

\* Email: 592082823@qq.com

ZigBee (Mohsin et al., 2017; Hui et al., 2015; Lian and Li, 2012), global system for mobile communications (GSM) (Rajput et al., 2013), and power line communication (PLC) (Liu et al., 2008). With automation functions added to the ISL control process, environmental protection, high system efficiency and energy conservation can be achieved, and sufficient lighting can be provided for late-night travellers (Deo et al., 2014).

Various studies have analysed the effect of using different communication strategies in ISL management systems. ZigBee is a short-range wireless network standard that uses the 2.4 GHz frequency band to achieve data transmission of up to 250 kbps (Bingöl et al., 2019). ZigBee operates in a mesh networking standard, which means each node in the grid is connected and can act as a transmitter and receiver at the same time (Bingöl et al., 2019; Gagliardi et al., 2020). Fan and Guo (2011) propose a ZigBee-based wireless sensing network for a street lighting system for energy conservation. Besides, a wireless street light control system based on the ZigBee network framework is studied (Jin et al., 2016). The method employs ZigBee communication to realise remote monitoring and achieves power adjustment and ON/OFF control functions. GSM is a long-range communication technology. When it is used in an ISL system, the microcontroller can control the on/off status of a street light by setting a time delay, and an update can be sent to a designated phone number (Caponetto et al., 2008). Moreover, Parekar and Dongre (2015) introduce a GSM-based ISL system to achieve remote monitoring and control of street lights. The microcontroller in this system is used to process the sampled data and transmit the results to the control centre through short message service (SMS). To realise cost-effective and reliable ways for users to remotely control street lights, the command is sent to the base station for night lighting through SMS, and then the user can obtain a successful initiate response (Khandagale et al., 2020). PLC is a technology that uses power cables as a data transmission medium. With the merits of low maintenance cost and wide coverage, the research of PLC-based ISL systems has attracted attention in recent years (Zhu et al., 2011). For example, a signal relay approach is employed in a PLC-based ISL system to overcome the insufficient distance of PLC, and management and timely control functions are realised through the effective use of grid resources (Xu et al., 2019). Liu et al. (2008) designed a homemade power modem chip to suppress noise in low voltage power lines, thereby ensuring the efficiency and reliability of the ISL remote control. Because of the simple signal modulation scheme and intense interference rejection capability, in some studies, switches are utilised to modulate and inject signals into power lines for communication between the central controller and each street light (Li et al., 2010; Bertoni et al., 2015).

Switching ripple communication (SRC) is a novel strategy that integrates communication information in harmonic of energy due to the high switching frequency of power electronics devices. Because SRC is a converter-based communication approach, it can be used in a wide range of applications that involve power electronics and require communication. For example, Chen et al. (2021) proposed a baseband SRC approach for LED lighting to realise high data rates and low switching frequencies. Moreover, Choi and Jung (2017) proposed SRC-based DC microgrids to promote power conversion efficiency and omit extra amplifiers and wires. In addition, a cascaded multilevel inverter was applied to an electric vehicle powertrain for battery balance, charging and discharging, and motor speed control (Zhang et al., 2020), where the state of charge of batteries and motor speed control signals are transmitted through the SRC method. As an alternative communication strategy to wireless and wired communication, SRC has the following merits. Firstly, the communication signals are modulated on the fixed power line, thus the SRC method has higher signal stability than wireless communication. Besides, the use of additional communication lines in wired communication can be avoided, thus simplifying the system structure, and reducing the cost. In terms of signal security, the wireless methods broadcast signals over the air, which is vulnerable to potential hackers, whereas in the SRC method, the signals are transmitted over physical cables, which is considered to be more secure. Compared to other wired communication methods such as RS-485, it is more difficult to invade the signal directly from the cable of the SRC method because the signal is integrated with energy.

A buck-boost converter-based ISL topology is proposed in this paper. The proposed model uses the SRC method for two-way communication between the central controller and each street light through the DC bus. Because the communication signal is modulated by the switching frequency of the buck-boost converter, the transmitted data is integrated into the current waveform and transmitted along with the power conversion. This model has the following advantages. Firstly, only minor modifications are applied to the conventional buck-boost converter to suit the street light application, making the model simple to implement. Secondly, the proposed model inherits the merit of conventional PLC communication that no additional wiring is required, and at the same time eliminates the requirement for signal coupling devices. Thirdly, compared to other research on the same application (Li et al., 2010; Bertoni et al., 2015), the proposed model uses an additional 'request to send (RTS)/confirm to send (CTS)' mechanism to reduce frame conflicts, thereby enabling effective remote street light control in the ISL system.

The remainder of this paper is organised as follows. In Section 2, the structure of the proposed ISL system is presented. In Section 3, the mechanisms of the proposed topology in charging and discharging modes are explained. Subsequently, the signal transmission method and the approach to avoid frame collision are shown in Section 4. In Section 5, the performance of the proposed method is evaluated in terms of bit error rate (BER) based on the simulation results. Finally, the conclusion is drawn in Section 6.

## 2. System Configuration

The proposed system model is presented in Figure 1. Each street light is equipped with a large-capacity battery to store energy from solar panels, and then the stored energy is used to power the LEDs at night. Solar panels are placed on the roof of the bus station platform, so solar energy can be collected without taking up too much platform space. Besides, each street light contains a monitor for monitoring street conditions. Furthermore, an electronic screen is placed on each street light to cycle through advertisements, news, and traffic information. Additionally, extra power generated by the solar panels can be used by passengers to charge electronic devices (Chu et al., 2017; Hu et al., 2013, 2014a). The battery in each street light can also be used to charge electric vehicles in emergencies such as large-scale power outages in cities (Hu et al., 2014b, 2015, 2017). Assuming that the power of each LED street light is 100 W, the distance between the two street lights is 40 m, and the average distance between two platforms is 800 m, then 20 LED street lights are required between two platforms, and the solar panel is required to generate at least 2 kW of power. If a 1.5 m<sup>2</sup>, 300 W solar panel is used to power the street lights, 7–8 such panels are required, covering an area of 10.5–12 m<sup>2</sup>. Therefore, it is feasible to place solar panels on top of a bus station.

The communication between the control centre and the street lights is realised by transmitting data through converters. Specifically, the LED status data such as voltage, current and temperature are first measured by relevant sensors. Then these data are modulated by the fast-switching switches of a DC/DC converter through microcontrollers. After transmitting these data through the DC bus, the data can be extracted, demodulated, and recovered from the current waveform at the control centre. Similarly, the LEDs' operating command from the control centre can be transmitted with the same modulation and demodulation approach. Through this two-way communication mode, the remote-control centre can rapidly update the working status of the LED lights and adjust the lighting plan according to the remaining power of the battery. Figure 2 presents the proposed buck-boost converter topology for the ISL application. The master node of the remote-control centre contains a battery as the DC power source for signal generation. The topology will operate as a buck converter during battery charging and a boost converter during battery discharging. Each LED branch contains a thermistor  $R_T$  for LED overcurrent protection.

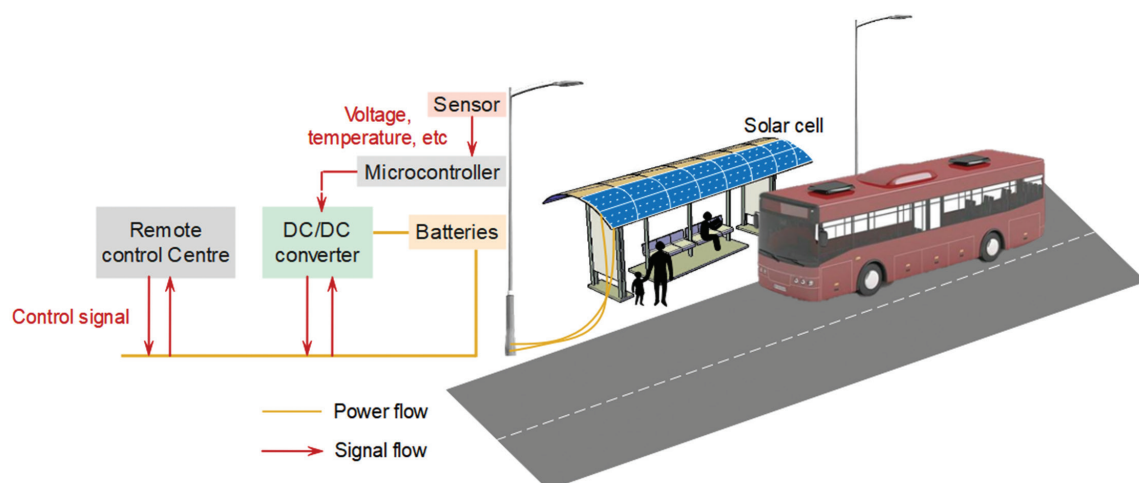


**Fig. 1.** Energy and signal flow of the proposed ISL system. ISL, intelligent street lighting.

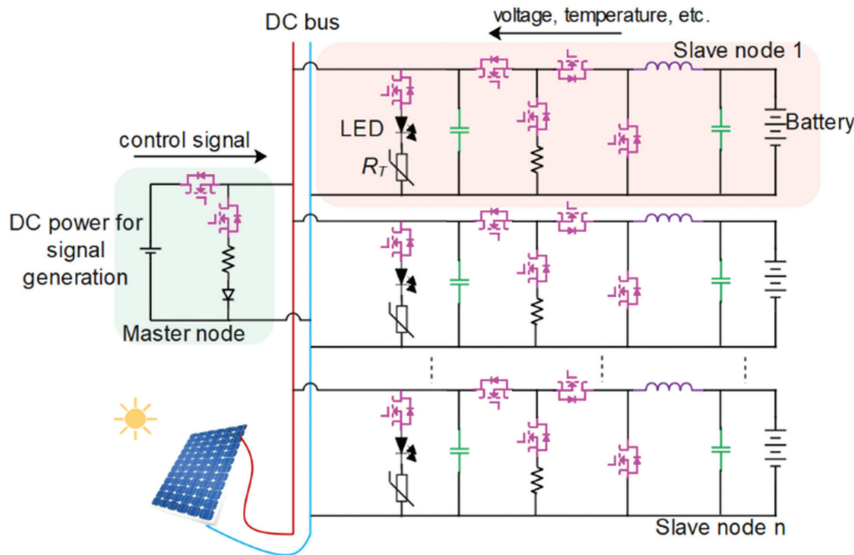


Fig. 2. The proposed buck-boost converter for the ISL system. ISL, intelligent street lighting; LED, light-emitting diode.

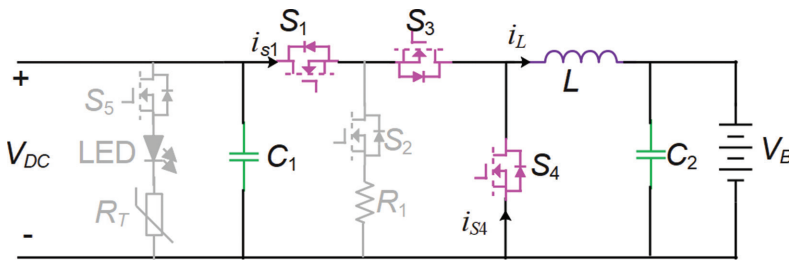


Fig. 3. Equivalent circuit of the proposed topology in charging mode. LED, light-emitting diode.

### 3. Operation Principle

#### 3.1. Charging mode

Figure 3 shows the equivalent circuit of the proposed topology in charging mode. Because various slave modules are charged with the same strategy, only one module is presented in Figure 3 as an example. Pulse width modulation (PWM) is used to control switch  $S_1$ . The typical waveforms are illustrated in Figure 4, where  $v_{gs1}$ ,  $i_L$ ,  $i_{S1}$  and  $i_{S4}$  refer to the conduction signal of switch  $S_1$ , the current flowing through inductor  $L$ , the current flowing through switch  $S_1$ , and the current flowing through switch  $S_4$ , respectively.

Assuming that all components are ideal, the stages of the proposed circuit in continuous conduction mode (CCM) are explained below:

- Stage 1* [ $t_0-t_1$ ]: Switch  $S_1$  is turned on, and switches  $S_3$  and  $S_4$  are turned off. The energy from the DC bus  $V_{DC}$  is transferred to inductor  $L$ , battery  $V_B$ , and capacitors  $C_1$  and  $C_2$ . The current flow direction is exhibited in Figure 5(a).
- Stage 2* [ $t_1-t_2$ ]: Switches  $S_1$ ,  $S_3$  and  $S_4$  are turned off. The energy stored in inductor  $L$  is transferred to battery  $V_B$  and capacitor  $C_2$ . The current flow direction is displayed in Figure 5(b).

In the steady state, because the initial value of the inductor current is equal to its final value, the voltage gain  $G_c$  is derived as

$$G_c = \frac{V_B}{V_{DC}} = D, \tag{1}$$

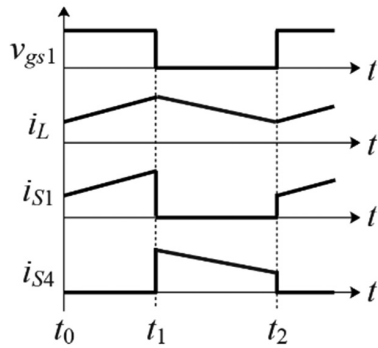


Fig. 4. The key waveforms of the proposed converter in charging mode.

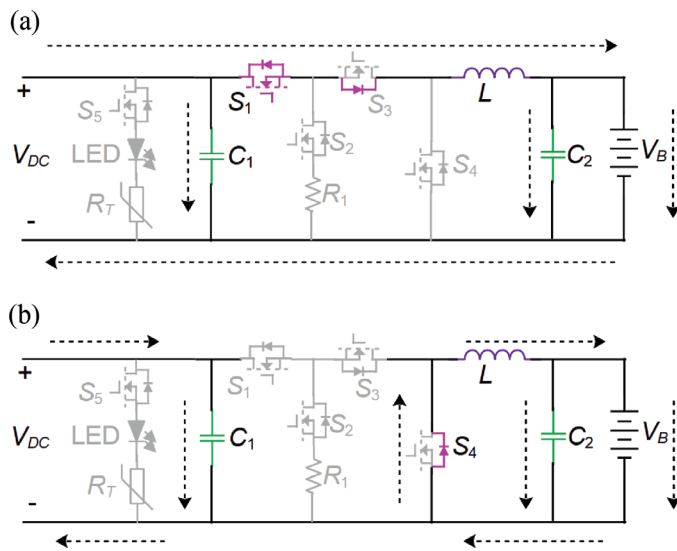


Fig. 5. The current direction (a)  $[t_0-t_1]$  and (b)  $[t_1-t_2]$  of the proposed topology in charging mode. LED, light-emitting diode.

where  $D$  is the duty ratio. The minimum inductor current  $I_{Lmin}$  can be calculated as

$$I_{Lmin} = I_O - \frac{V_B}{2L}(1-D) \cdot T_s, \tag{2}$$

where  $I_o$  is the output current, and  $T_s$  is the switching period. Because the minimum inductor current is zero at the boundary condition, the value of inductor  $L$  can be obtained from

$$L = \frac{(1-D)}{2f_s} \cdot R_B, \tag{3}$$

where  $R_B$  is the equivalent load on the battery side, and  $f_s$  is the switching frequency. The inductor is designed to be larger than this boundary value to ensure the circuit operates in CCM mode.

### 3.2. Discharging mode

Figure 6 shows the equivalent circuit of the proposed topology in discharging mode. Switch  $S_5$  is turned on, and the PWM method is used to control switches  $S_3$  and  $S_4$ . Some typical waveforms are illustrated in Figure 7, where  $v_{gs3}$ ,  $v_{gs4}$ ,  $i_L$ ,  $i_{S3}$ , and  $i_{S4}$  respectively represent the conduction signal of switch  $S_3$ , the conduction signal of switch  $S_4$ , the current flowing through inductor  $L$ , the current flowing through switch  $S_3$ , and the current flowing through switch  $S_4$ .

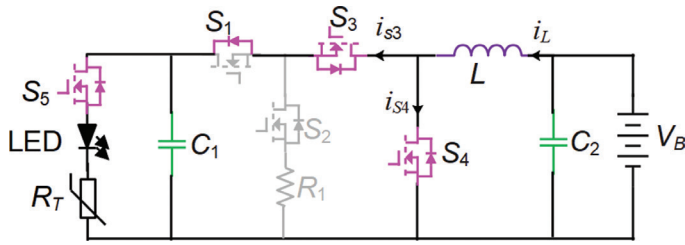


**Fig. 6.** Equivalent circuit of the proposed topology in discharging mode. LED, light-emitting diode.

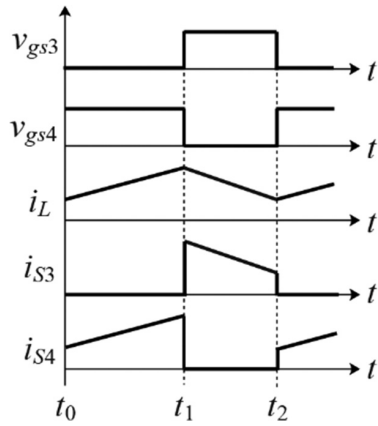
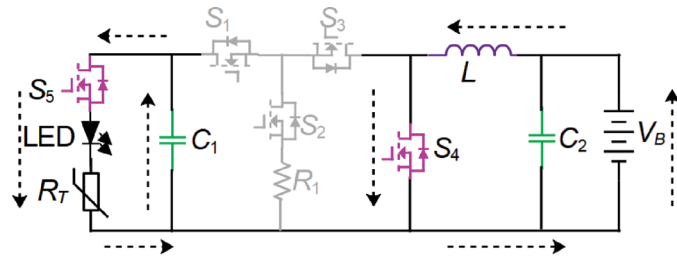
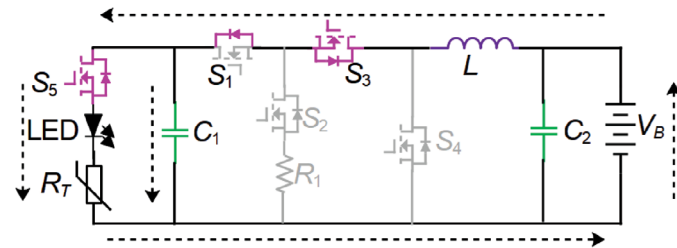


**Fig. 7.** The key waveforms of the proposed converter in discharging mode.



(a)



(b)

**Fig. 8.** The current direction (a)  $[t_0 - t_1]$  and (b)  $[t_1 - t_2]$  of the proposed topology in discharging mode. LED, light-emitting diode.

The stages of the proposed circuit in CCM mode are presented below.

*Stage 1  $[t_0 - t_1]$ :* Switch  $S_4$  is turned on, and switches  $S_1$  and  $S_3$  are turned off. Inductor  $L$  is charged by battery  $V_B$ , and the energy stored in capacitor  $C_1$  is transferred to the LED. The current flow direction is shown in Figure 8(a).

**Stage 2** [ $t_1$ – $t_2$ ]: Switch  $S_4$  is turned off, and switch  $S_3$  is turned on. The energies stored in inductor  $L$  and battery  $V_B$  are discharged to the LED and capacitor  $C_1$ . The current flow direction is presented in Figure 8(b).

Because the current increment and current reduction of inductor  $L$  are equal in one cycle, the voltage gain  $G_d$  can be acquired as

$$G_d = \frac{V_O}{V_B} = \frac{1}{1-D}, \quad (4)$$

where  $V_O$  is the output voltage. The inductor boundary current  $I_{LB}$  is derived as

$$I_{LB} = \frac{1}{2} \cdot \frac{V_B}{L} \cdot DT_S = \frac{V_B}{2Lf_s} \cdot D. \quad (5)$$

Since the output current  $I_O$  is equal to the inductor current when switch  $S_4$  is turned off, the output boundary current  $I_{OB}$  can be obtained from

$$I_{OB} = I_{LB} \cdot (1-D) = \frac{V_O}{2Lf_s} \cdot D(1-D)^2. \quad (6)$$

The minimum value of inductor  $L$  can be calculated from

$$L_{min} = \frac{RD(1-D)^2}{2f_s}, \quad (7)$$

where  $R$  is the equivalent load on the LED side. After comparing the boundary value of the inductor in the charging and discharging modes, the inductor suitable for the proposed model can be determined. In other words, the selected inductance is greater than the maximum inductance boundary value of these two operating modes.

## 4. Data Transmission Mechanisms

### 4.1. Modulation and demodulation

The Fourier series expression of a typical PWM waveform with amplitude  $A$  and period  $T$  in Figure 9 is shown in Eq. (8), and the Fourier coefficients of Eq. (8) are presented in Eq. (9).

$$f(x) = a_0 + \sum_{n=1}^{\infty} (a_n \cos n\omega t + b_n \sin n\omega t) \quad (8)$$

$$\begin{cases} a_0 = DA \\ a_n = \frac{2A}{\pi n} \sin(\pi Dn) \cos(\pi Dn) \\ b_n = \frac{2A}{\pi n} \sin^2(\pi Dn) \\ c_n = \sqrt{a_n^2 + b_n^2} = \frac{2A}{\pi n} |\sin(\pi Dn)| \end{cases} \quad (9)$$

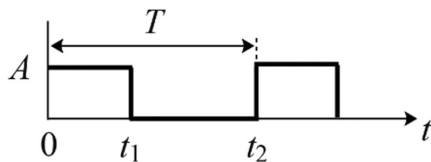


**Fig. 9.** A typical PWM waveform. PWM, pulse width modulation.

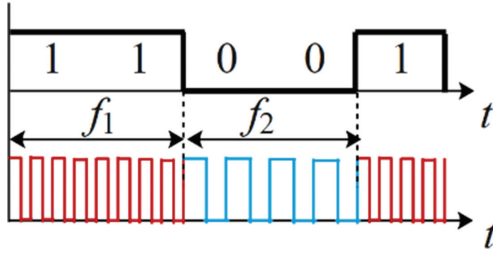


**Fig. 10.** FSK method for signal modulation. FSK, frequency shift keying.

In Eqs (8) and (9), the angular frequency of the typical waveform is represented by  $\omega$ , and the duty ratio  $D$  is related to period  $T$ . The amplitude of high-frequency components  $c_n$  indicates that these components exist during the power conversion process and can be reasonably employed as carriers for data transmission. In the proposed system, the combined frequency shift keying (FSK) and PWM approach are used for both energy and signal transmission. As shown in Figure 10, carriers with frequency  $f_1$  and  $f_2$  are utilised to modulate digital '1' and digital '0', respectively. When the transmission channel is idle, only frequency  $f_2$  is used for energy conversion with the PWM method.

To ensure the utilised carriers are orthogonal to each other, the minimum carrier spacing  $\Delta f$  is obtained from

$$\Delta f = \frac{1}{T_U}, \quad (10)$$

where  $T_U$  is the time used for transmitting a single bit of data. After the signal is transmitted through the DC bus, the carrier can be demodulated from the current waveform using a band-pass filter. The sampling frequency  $f_{sample}$  of the band-pass filter is set to be greater than twice the upper limit frequency  $f_{cut}$  of the passband based on the Nyquist theorem

$$f_{sample} > 2f_{cut}. \quad (11)$$

Presume that the demodulated carrier at the receiver is

$$x(t) = A_1 \cos(2\pi f_1 t + \theta_1) [1 - y(t)] + A_n \cos(2\pi f_n t + \theta_n), \quad (12)$$

where

$$y(t) = \begin{cases} 1, & \text{if digital '0' is sent or the channel is idle} \\ 0, & \text{if digital '1' is sent} \end{cases}. \quad (13)$$

In Eq. (12), the demodulated carrier is simplified as the combination of demodulated carrier and noise, where  $A_1$  refers to the amplitude of the carrier's first-order harmonic, and  $A_n$  is the superimposed amplitude of other harmonics. Then the Hilbert transform approach is applied to extract the envelope  $e(t)$  of the demodulated carrier

$$\begin{cases} e(t) = \sqrt{x(t)^2 + \hat{x}(t)^2} \\ \hat{x}(t) = \frac{1}{\pi} \int_{-\infty}^{\infty} \frac{x(\tau)}{t - \tau} d\tau \end{cases}. \quad (14)$$

Because the amplitude of other order harmonics is greatly suppressed after the filtering process, a threshold value  $V_{th}$  is used to further separate the carrier-envelope from the noise envelope, where the range of  $V_{th}$  is selected between

$$A_n < V_{th} < A_1. \quad (15)$$

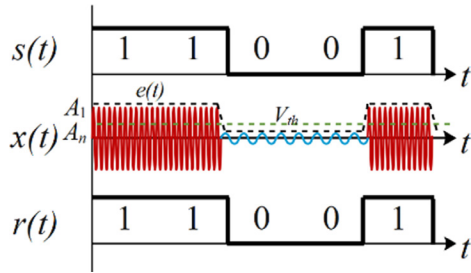


Fig. 11. The typical waveforms during the demodulation process.

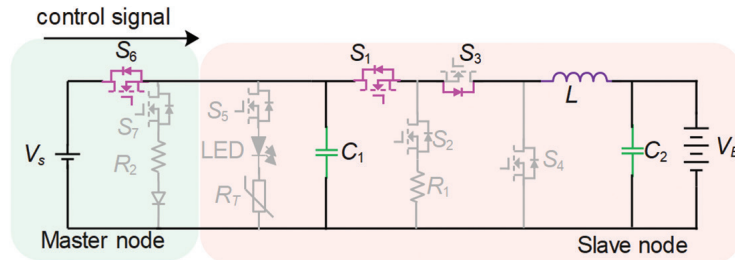


Fig. 12. Equivalent circuit when the master node is transmitting signals. LED, light-emitting diode.

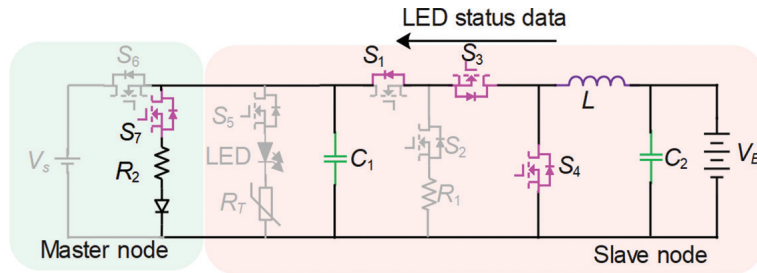


Fig. 13. Equivalent circuit when the slave node is transmitting signals. LED, light-emitting diode.

Finally, the transmitted signal is recovered by resampling the extracted envelope with the initial data transmission rate. The signal demodulation process is exhibited in Figure 11, where  $s(t)$ ,  $x(t)$  and  $r(t)$  refer to the initial signal, demodulated carrier waveform and recovered signal, respectively.

## 4.2. Bidirectional communication

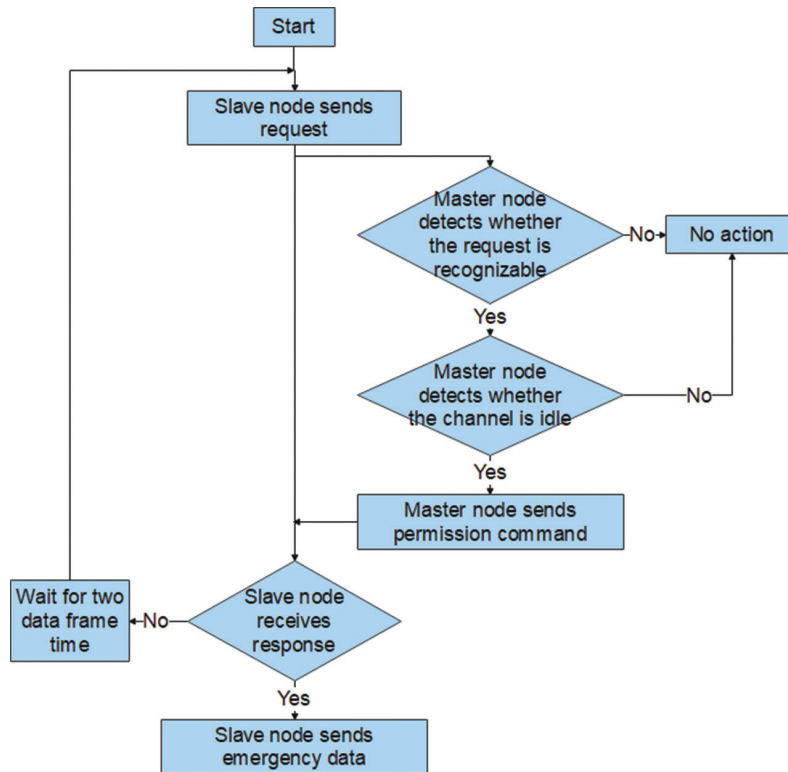
Figure 12 shows the equivalent circuit of the proposed topology when the master node transmits control signals to a slave node. This topology is similar to the topology in the charging mode explained in Section 3, both of which can be regarded as buck converters. The difference is that switch  $S_6$  is utilised for signal modulation at the master node, switch  $S_1$  is turned on to guide the signal to the slave node, and capacitor  $C_1$  is involved in the discharging path of inductor  $L$ .

Figure 13 shows the equivalent circuit of the proposed topology when a slave node transmits LED status data to the master node. This topology is like that of the topology in discharging mode described in Section 3, which utilises switches  $S_3$  and  $S_4$  for signal modulation. Furthermore, switch  $S_7$  is turned on to guide the signal to the master node. The topology shown in Figure 13 can be considered as a boost converter.

The data frame structure is defined in Table 1. An 8-bit preamble is introduced at the beginning of each frame to synchronise the sender and receiver. Each LED has a unique ID number, which is employed to identify the source/destination address of the information. Check codes are added at the end of each data string to verify whether the data are damaged during transmission. Finally, an 8-bit end code is appended to the end of each frame to indicate

**Table 1.** Structure of one data frame

Code type	Preamble	Node ID	Data	Check code	Ending character
Length (bits)	8	8	0–64	8	8


**Fig. 14.** Flowchart of the emergency data transmission mechanism.

frame termination. In this case, each frame contains data/commands for a single LED, and various LED data/commands are sent frame by frame according to the node ID sequence.

### 4.3. Emergency signal transmission

Although the system can periodically transmit LED status data, emergency communication with personnel in the remote-control centre is essential to handle emergencies (such as bulb failure). The emergency communication strategy of the proposed system is shown in Figure 14.

Firstly, a slave node sends a frame of 'RTS' signal to the master node to inform the master node of the data transmission action it will perform. Secondly, the master node receives the RTS signal and detects whether the communication channel is idle. Specifically, if digital '1' is demodulated within the time of the next data frame, the master node will presume that the channel is busy and will not respond. Otherwise, the master node will presume that the channel is idle and send a frame of 'CTS' signal to the slave node to approve the request. Finally, if the slave node receives the CTS signal within two cycles of the data frame, it will transmit the emergency data. Otherwise, it will postpone time  $T_p$  to resend the RTS signal

$$T_p = T_s \cdot N, (N \in [0, 1, 2, \dots, n]), \quad (16)$$

where  $T_s$  is the time spent on transmitting a data frame,  $n$  is the number of slave nodes, and  $N$  is a random integer used to delay the sending time of the RTS signal. The carrier frequency different from the modulated data frame is used to modulate the digital '1' of the RTS and CTS signals so that the data frame and the RTS frame vary in

**Table 2.** Structure of the RTS/CTS signal

Code type	Preamble	Node ID	Check code	Ending character
Length (bits)	2	8	2	2

CTS, confirm to send; RTS, request to send.

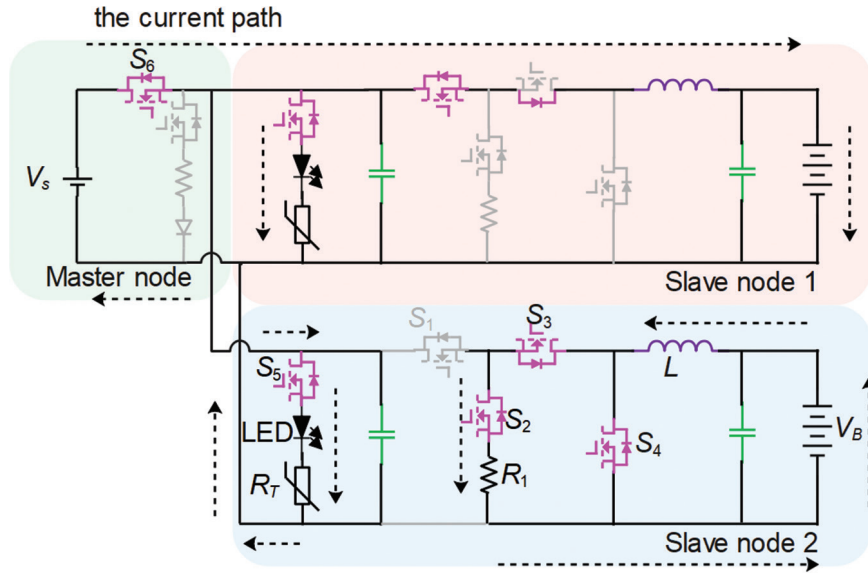


**Fig. 15.** The equivalent circuit when the master node is transmitting a CTS signal to slave node 1. CTS, confirm to send; LED, light-emitting diode.

frequency. Table 2 shows the frame structure of the RTS and CTS signals. Since the packets of RTS and CTS are very small, the overall transmission overhead will not dramatically increase. Furthermore, since the carrier of the same frequency is used to modulate the RTS signal, the node ID demodulated at the master node does not correspond to the actual node address when multiple slave nodes send requests at the same time. The master node does not send any response in this case. Therefore, it is ensured that when one node sends data, other nodes will not use the channel to avoid conflicts.

The voltage value of source  $V_s$  at the master node is designed to be greater than the battery voltage  $V_b$  to ensure that the transmitted CTS signal can be received at the slave node. The equivalent circuit of this scenario is presented in Figure 15. In this figure, the master node is sending a CTS signal to slave node 1. Slave node 1 is working in charging mode and slave node 2 is operating in discharging mode. The LED lights are powered by the power source of the master node. Switches  $S_2$  and  $S_3$  are turned on during the period when switch  $S_4$  is turned off to release the charge stored in inductor  $L$ .

## 5. Results and Analysis

### 5.1. Simulation results

A simulation model is implemented in MATLAB/Simulink to examine the feasibility of the proposed system. Table 3 presents the system parameters used in the simulation model, where the switching frequencies are chosen as  $f_1 = 30$  kHz,  $f_2 = 20$  kHz, and  $f_3 = 50$  kHz. The data rate is 2 kbps in the simulation model. Besides, the resistance of the thermistor  $R_T$  under normal conditions is  $10 \Omega$ . Some typical simulation waveforms of a slave node operating in charging mode and discharging mode are presented in Figures 16 and 17, respectively. The currents flowing through the switches  $S_1$ ,  $S_3$  and  $S_4$  are represented by  $i_{S1}$ ,  $i_{S3}$  and  $i_{S4}$ , respectively. Moreover,  $i_L$ ,  $V_b$  and  $V_o$  respectively refer to the inductor current, battery side voltage, and output voltage at the LED side. It can be observed from the simulation results that the designed topology operates in CCM mode as expected.

**Table 3.** Parameter specifications of the simulation model

Parameter name	Value
$V_{DC}$ (DC bus voltage)	20 V
$V_B$ (battery voltage)	12 V
$V_O$ (output voltage of discharging mode)	15 V
$V_S$ (source voltage at the master node)	20 V
$L$ (inductor at slave node)	3 mH
$C_1, C_2$ (capacitor at slave node)	100 $\mu$ F
$R_T$ (thermistor)	10 $\Omega$
$P_{out1}$ (output power of a slave node at charging mode)	18 W
$P_{out2}$ (output power of a slave node at discharging mode)	15 W
$f_1$ (frequency for modulating '1' of a data frame)	30 kHz
$f_2$ (frequency for modulating '0' or normal switching frequency)	20 kHz
$f_3$ (frequency for modulating '1' of an RTS/CTS frame)	50 kHz
$f_{sample}$ (sampling frequency of the band-pass filter)	120 kHz
$T_U$ (one-bit data time)	500 $\mu$ s

CTS, confirm to send; RTS, request to send.

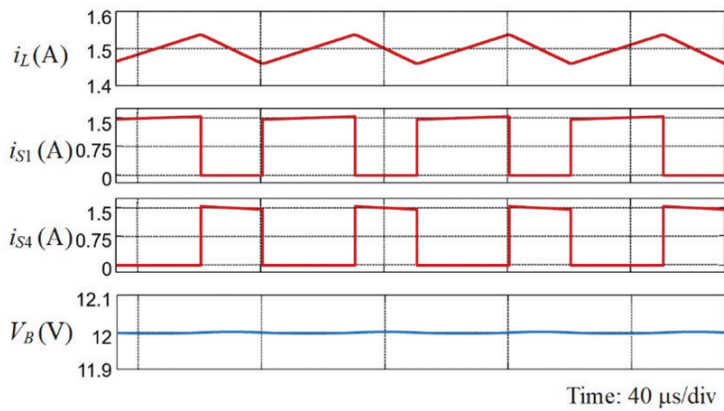


**Fig. 16.** The typical waveforms of the proposed topology operate in charging mode.

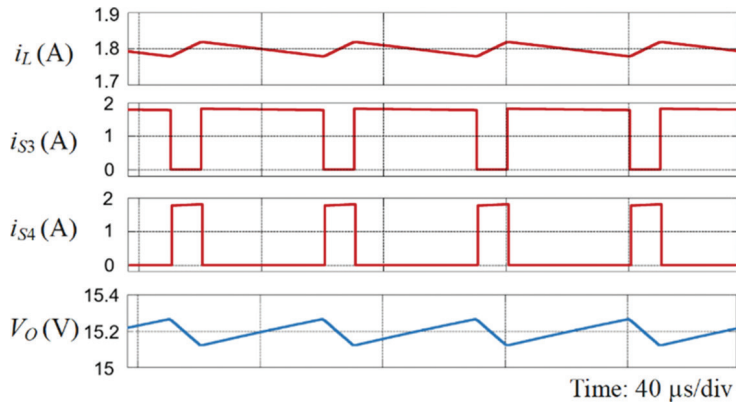


**Fig. 17.** The typical waveforms of the proposed topology operate in discharging mode.

Figures 18 and 19 respectively exhibit the key waveforms of the master node transmitting signals to slave nodes and slave nodes sending signals to the master node. Three slave nodes are connected to the master node in the simulation model, and these slave nodes transmit data in sequence based on their ID numbers. When one slave

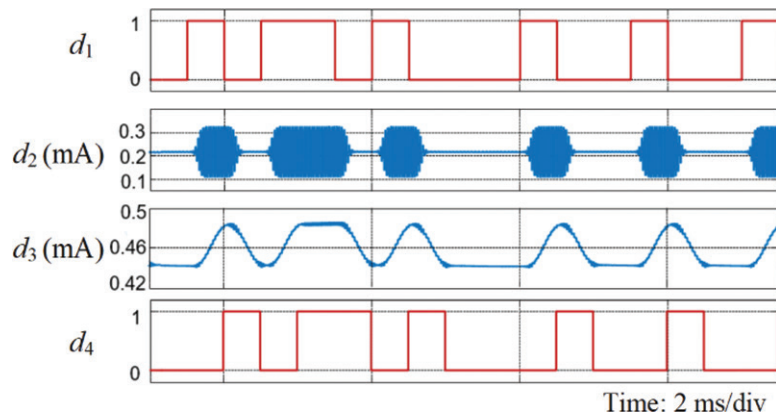


**Fig. 18.** The typical waveforms when the master node transmits a signal.

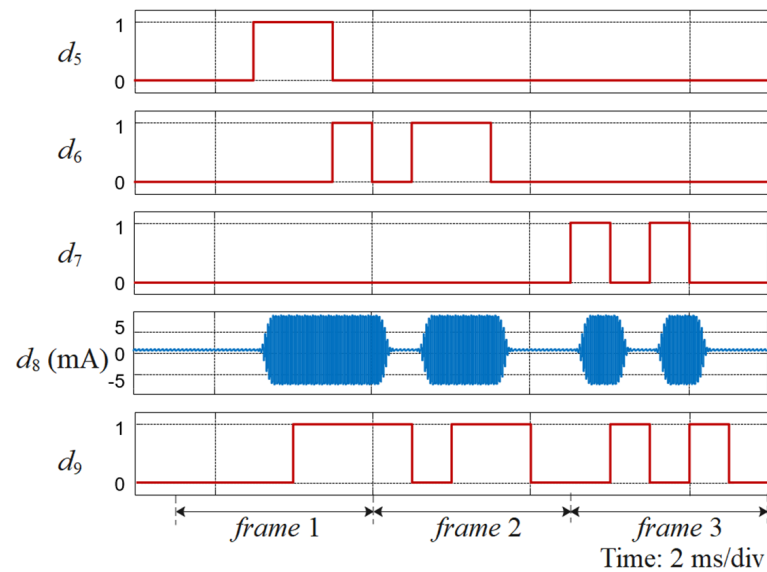


**Fig. 19.** The typical waveforms when the slave nodes transmit signals.

node sends data, the other two nodes will operate normally and supply power to the LED. In Figure 18,  $d_1$ ,  $d_2$ ,  $d_3$  and  $d_4$  respectively represent the original signal, demodulated carrier of digital '1', extraction amplitude of the first-order harmonic and restored signal. In Figure 19,  $d_5$ ,  $d_6$ ,  $d_7$ ,  $d_8$  and  $d_9$  respectively represent data frame from slave node 1, data frame from slave node 2, data frame from slave node 3, demodulated carrier of digital '1' and restored signal at the master node. Figure 20 presents the result when a slave node receives a CTS signal from the master node, where  $d_{10}$ ,  $d_{11}$ ,  $d_{12}$  and  $d_{13}$  refer to the original signal, demodulated carrier of digital '1', extraction amplitude of the first-order harmonic, and restored signal, respectively. It can be observed that a one-bit delay occurs at the receiver, which is mainly caused by the filtering process and re-sampling at the original signal rate. The successfully restored signal proves the feasibility of utilising the SRC method in the ISL system. Besides, it is possible to use the switching ripple to transmit RTS/CTS signals for data frame collision reduction.

## 5.2. Noise immunity analysis

The noise immunity of the proposed model is analysed by introducing white Gaussian noise to the power line as environmental interference. The BER is calculated by comparing the transmitted and received data bit by bit. The relationship between BER and the signal-to-noise ratio (SNR) is then derived by gradually increasing the noise intensity. The simulation result is shown in Figure 21. The result indicates that the BER decreases as the SNR

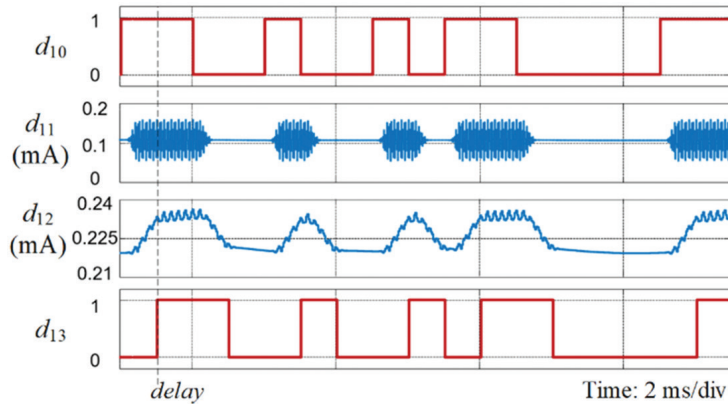


**Fig. 20.** The typical waveforms when the master node transmits a CTS signal. CTS, confirm to send.

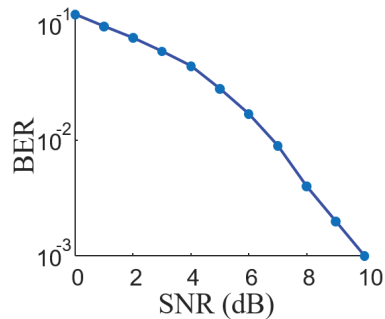


**Fig. 21.** The relationship between BER and SNR. BER, bit error rate; SNR, signal-to-noise ratio.

increases and the proposed SRC method has decent anti-noise ability. Specifically, the BER is  $<10^{-3}$  when the SNR is  $>10$  dB with a data rate of 2 kbit/s.

## 6. Conclusions

In this paper, a bidirectional buck-boost converter topology is presented for realising two-way communication in an ISL system. The transmitted energy is modulated by the PWM method, and the transmitted signal is modulated by the FSK approach. The battery in each street light is charged during the day and powers the LEDs at night. The remote-control centre can transmit LED control signals and collect LED status data in this model. Because the transmission signals are integrated into the current waveform by modulating the switching frequency, the cost of system wiring can be reduced. Moreover, the adopted RTS/CTS communication scheme can greatly reduce the conflict of emergency signals. The simulation model established in MATLAB/Simulink proves the feasibility of this method in the ISL system. Furthermore, the noise immunity is analysed at a data rate of 2 kbit/s. When the SNR is  $>10$  dB, a BER of  $<10^{-3}$  can be achieved.

## References

- Adriansyah, A., Dani, A. W. and Nugraha, G. I. (2017). Automation Control and Monitoring of Public Street Lighting System Based on Internet of Things. In *2017 International Conference on Electrical Engineering and Computer Science (ICECOS)*. Palembang, Indonesia. IEEE, pp. 231–236.
- Bertoni, N., Bocchi, S., Mangia, M., Pareschi, F., Rovatti, R. and Setti, G. (2015). Ripple-based Power-line

- Communication in Switching DC-DC Converters Exploiting Switching Frequency Modulation. In *2015 IEEE International Symposium on Circuits and Systems (ISCAS)*. Lisbon, Portugal. IEEE, pp. 209–212.
- Bingöl, E., Gül, Ö. and Şener, S. (2019). A Review of Intelligent Street Lighting System for Smart Cities. In *2nd International Symposium on Multidisciplinary Studies and Innovative Technologies*.
- Caponetto, R., Dongola, G., Fortuna, L., Riscica, N. and Zufacchi, D. (2008). Power Consumption Reduction in a Remote Controlled Street Lighting System. In *2008 International Symposium on Power Electronics, Electrical Drives, Automation and Motion*. Ischia, Italy. IEEE, pp. 428–433.
- Chen, J., Wu, J., Wang, R., Zhang R. and He, X. (2021). Coded PWM Based Switching Ripple Communication Applied in Visible Light Communication. *IEEE Transactions on Power Electronics*, 36(8), pp. 9659–9667.
- Choi, H. J. and Jung, J. H. (2017). Enhanced Power Line Communication Strategy for DC Microgrids Using Switching Frequency Modulation of Power Converters. *IEEE Transactions on Power Electronics*, 32(6), pp. 4140–4144.
- Chu, G., Wen, H., Jiang, L., Hu, Y. and Li, X. (2017). Bidirectional Flyback Based Isolated-port Submodule Differential Power Processing Optimizer for Photovoltaic Applications. *Solar Energy*, 158, pp. 929–940.
- Deo, S., Prakash, S. and Patil, A. (2014). Zigbee-based Intelligent Street Lighting System. In *2014 2nd International Conference on Devices, Circuits and Systems (ICDCS)*. Coimbatore, India. IEEE, pp. 1–4.
- du Toit, P., Kruger, C., Hancke, G. P. and Ramotsoela, T. D. (2017). Smart Street Lights Using Power Line Communication. In *2017 IEEE AFRICON*. Cape Town, South Africa. IEEE, pp. 1581–1586.
- Fan, C. L. and Guo, Y. (2011). The Application of a ZigBee Based Wireless Sensor Network in the LED Street Lamp Control System. In *2011 International Conference on Image Analysis and Signal Processing*. Wuhan, China. IEEE, pp. 501–504.
- Gagliardi, G., Lupia, M., Cario, G., Tedesco, F., Gaccio, F. C., Lo Scudo, F. and Casavola, A. (2020). Advanced Adaptive Street Lighting Systems for Smart Cities. *Smart Cities*, 3(4), pp. 1495–1512.
- Gu, Z., Yang, K., Wang, X. and Meng, Q. (2018). Design of DC Charging Pile Based on Intelligent LED Lamp Rod. In *International Conference on Mechatronics and Intelligent Robotics*. Springer, Cham, pp. 916–922.
- Hu, Y., Gao, B., Song, X., Tian, G. Y., Li, K. and He, X. (2013). Photovoltaic Fault Detection Using a Parameter Based Model. *Solar Energy*, 96, pp. 96–102.
- Hu, Y., Cao, W., Finney, S. J., Xiao, W., Zhang, F. and McLoone, S. F. (2014a). New Modular Structure DC–DC Converter Without Electrolytic Capacitors for Renewable Energy Applications. *IEEE Transactions on Sustainable Energy*, 5(4), pp. 1184–1192.
- Hu, Y., Song, X., Cao, W. and Ji, B. (2014b). New SR Drive With Integrated Charging Capacity for Plug-in Hybrid Electric Vehicles (PHEVs). *IEEE Transactions on Industrial Electronics*, 61(10), pp. 5722–5731.
- Hu, Y., Gan, C., Cao, W., Li, C. and Finney, S. J. (2015). Split Converter-fed SRM Drive for Flexible Charging in EV/HEV Applications. *IEEE Transactions on Industrial Electronics*, 62(10), pp. 6085–6095.
- Hu, Y., Gan, C., Sun, Q., Li, P., Wu, J. and Wen, H. (2017). Modular Tri-port High-power Converter for SRM Based Plug-in Hybrid Electrical Trucks. *IEEE Transactions on Power Electronics*, 33(4), pp. 3247–3257.
- Hui, Z. X., Hua, K. P., Xu, Z. and Yang, L. (2015). Intelligent Street Lamp Energy Saving System Based on ZigBee. In *2015 Fifth International Conference on Instrumentation and Measurement, Computer, Communication and Control (IMCCC)*. Qinhuangdao, China. IEEE. pp. 786–789.
- Jin, D., Hannon, C., Li, Z., Cortes, P., Ramaraju, S., Burgess, P., Buch, N. and Shahidehpour, M. (2016). Smart Street Lighting System: A Platform for Innovative Smart City Applications and a New Frontier for Cyber-security. *The Electricity Journal*, 29(10), pp. 28–35.
- Khandagale, H. P., Zambare, R., Pawar, P., Jadhav, P., Patil, P. and Mule, S. (2020). Street Light Controller with GSM Technology. *International Journal of Engineering Applied Sciences and Technology*, 4(10), pp. 268–271.
- Li, C., Wu, J. and He, X. (2010). Realization of a General LED Lighting System Based on a Novel Power Line Communication Technology. In *2010 Twenty-Fifth Annual IEEE Applied Power Electronics Conference and Exposition (APEC)*. Palm Springs, CA, USA. IEEE, pp. 2300–2304.
- Lian, L. and Li, L. (2012). Wireless Dimming System for LED Street Lamp Based on ZigBee and GPRS. In *2012 3rd International Conference on System*

- Science, Engineering Design and Manufacturing Informatization*. Chengdu, China. IEEE, pp. 100–102.
- Liu, J., Feng, C., Suo, X. and Yun, A. (2008). Street Lamp Control System Based on Power Carrier Wave. In *2008 International Symposium on Intelligent Information Technology Application Workshops*. Shanghai, China. IEEE, pp. 184–188.
- Mohsin, M. M., Jadhav, I. S. and Chaudhari, V. D. (2017). High Efficiency Intelligent Street Lighting System Using a Zigbee Network and GSM. *International Journal for Research in Applied Science and Engineering Technology*, 5(2), pp. 510–516.
- Novak, T., Pollhammer, K., Zeilinger, H. and Schaat, S. (2014). Intelligent Streetlight Management in a Smart City. In *Proceedings of the 2014 IEEE Emerging Technology and Factory Automation (ETFA)*. Barcelona, Spain. IEEE, pp. 1–8.
- Parekar, S. R. and Dongre, M. M. (2015). An Intelligent System for Monitoring and Controlling of Street Light Using GSM Technology. In *2015 International Conference on Information Processing (ICIP)*. Pune, India. IEEE, pp. 604–609.
- Rajput, K. Y., Khatav, G., Pujari, M. and Yadav, P. (2013). Intelligent Street Lighting System Using GSM. *International Journal of Engineering Science Invention*, 2(3), pp. 60–69.
- SEA. Efficient Public Lighting Guide. (2012). Available at: [http://www.cityenergy.org.za/uploads/resource\\_17.pdf](http://www.cityenergy.org.za/uploads/resource_17.pdf). [Accessed 7 Mar. 2021].
- Xu, X., Zhan, A. and Li, X. (2019). Design and Implementation of Street Light Control System Based on Power Line Carrier Communication. *Procedia Computer Science*, 155, pp. 734–739.
- Zhang, Y., Chen, G., Hu, Y., Gong, C. and Wang, Y. (2020). Cascaded Multilevel Inverter Based Power and Signal Multiplex Transmission for Electric Vehicles. *CES Transactions on Electrical Machines and Systems*, 4(2), pp. 123–129.
- Zhu, E., Liu, X. and Aliaosha, Y. (2011). Development and Application of Low Voltage Power Line Communication Test System. In *2011 International Conference on Advanced Power System Automation and Protection*. Beijing, China. IEEE, pp. 320–322.